

# Geochemistry, Geophysics, Geosystems®

## RESEARCH ARTICLE

10.1029/2023GC011350

### Special Section:

Advances and Best Practices in  
Boron-based paleo-CO<sub>2</sub>  
reconstruction

### Key Points:

- Optimized method for B purification for  $\delta^{11}\text{B}$  analysis by multi-collector inductively coupled plasma mass spectrometry
- Allows faster sample processing (24 samples in ~5 hr)
- Minimizes procedural blanks (typically <20 pg)

### Supporting Information:

Supporting Information may be found in the online version of this article.

### Correspondence to:

M. Trudgill,  
molly.trudgill@lsce.ipsl.fr

### Citation:

Trudgill, M., Nuber, S., Block, H. E., Crumpton-Banks, J., Jurikova, H., Little, E., et al. (2024). A simple, low-blank batch purification method for high-precision boron isotope analysis. *Geochemistry, Geophysics, Geosystems*, 25, e2023GC011350. <https://doi.org/10.1029/2023GC011350>






Received 13 NOV 2023

Accepted 15 FEB 2024

© 2024 The Authors. *Geochemistry, Geophysics, Geosystems* published by Wiley Periodicals LLC on behalf of American Geophysical Union.

This is an open access article under the terms of the [Creative Commons Attribution License](#), which permits use, distribution and reproduction in any medium, provided the original work is properly cited.

## A Simple, Low-Blank Batch Purification Method for High-Precision Boron Isotope Analysis

M. Trudgill<sup>1,2</sup> , S. Nuber<sup>1,3</sup>, H. E. Block<sup>1</sup>, J. Crumpton-Banks<sup>1</sup>, H. Jurikova<sup>1</sup>, E. Little<sup>1,4</sup> , M. Shankle<sup>1</sup> , C. Xu<sup>1</sup> , R. C. J. Steele<sup>1</sup>, and J. W. B. Rae<sup>1</sup> 

<sup>1</sup>School of Earth and Environmental Sciences, University of St Andrews, St Andrews, UK, <sup>2</sup>Laboratoire des Sciences du Climat et de l'Environnement (LSCE/IPSL), Saint Aubin, France, <sup>3</sup>National Taiwan University, Taipei, Taiwan, <sup>4</sup>Institut de Ciència i Tecnologia Ambiental, (ICTA), Universitat Autònoma de Barcelona (UAB), Barcelona, Spain

**Abstract** Boron (B) isotopes are widely used in the Earth sciences to trace processes ranging from slab recycling in the mantle to changes in ocean pH and atmospheric CO<sub>2</sub>. Boron isotope analysis is increasingly achieved by multi-collector inductively coupled plasma mass spectrometry, which requires separation of B from the sample matrix. Traditional column chromatography methods for this separation have a well-established track record but are time consuming and prone to contamination from airborne blank. Here, we present an extensive array of tests that establish a novel method for B purification using a batch method. We discuss the key controls and limitations on sample loading, matrix removal and B elution including sample volume, ionic strength, buffer to acid ratio and elution volume, all of which may also help optimize column-based methods. We find consistent, low procedural blanks of  $10 \pm 16$  pg and excellent reproducibility: 10 ng NIST RM 8301 foram [8301f] yields  $14.58 \pm 0.11\%$  2SD  $n = 15$ ; 2.5 ng 8301f yields  $14.60 \pm 0.19\%$  2SD,  $n = 31$ ; and overall long term 2SD on  $n = 218$  samples pooling different sample sizes yields  $14.62 \pm 0.21\%$  2SD. This method also offers significant advantages in throughput, allowing the processing of 24 samples in ~5 hr. This boron batch method thus provides a fast, reproducible, low-blank method for purification of boron for high precision isotopic analyses.

## 1. Introduction

Boron (B) isotopes are increasingly used in the Earth Sciences, with applications including reconstruction of ocean pH and atmospheric CO<sub>2</sub> (e.g., Foster & Rae, 2016; Hönisch et al., 2019; Vengosh et al., 1991), tracking of biomineralization fluid chemistry in calcifiers (e.g., Allison et al., 2018; Gagnon et al., 2021), tracing of processes surrounding subduction and slab recycling (e.g., De Hoog & Savov, 2017), wastewater management, and weathering (Ercolani et al., 2019; Kloppmann et al., 2008; Muttik et al., 2011; Wei et al., 2015). Despite this, the wider application and resolution of B isotopes as a geochemical tool is limited by the time consuming nature and exacting requirements of current laboratory procedures. Early studies measured  $\delta^{11}\text{B}$  by thermal ionization mass spectrometry (TIMS, Hemming & Hanson, 1994; Zeininger & Heumann, 1983) which is typically achieved without chemical purification (Foster et al., 2013), but with limits on accuracy and sample throughput. The development of multi-collector inductively coupled plasma mass spectrometry (MC-ICPMS) techniques for  $\delta^{11}\text{B}$  analysis has helped improve reproducibility between laboratories (Gutjahr et al., 2020; Stewart et al., 2021) but requires the separation of B from its CaCO<sub>3</sub> matrix to avoid the impact of matrix-induced variability on analysis. Several different approaches to this have been explored, including microsublimation (Misra et al., 2014) and a batch method for large samples (>40 ppm, Douville et al., 2010; Lécuyer et al., 2002), with column chromatography being the most widely used method (Foster, 2008; Lemarchand et al., 2002; McCulloch et al., 2014). Boron purification is typically achieved using a gravimetric microcolumn filled with Amberlite IRA-743 resin (Lemarchand et al., 2002). This resin binds borate ion (B(OH)<sub>4</sub><sup>-</sup>) but not boric acid (B(OH)<sub>3</sub>) allowing the loading of B onto the resin at high pH as B(OH)<sub>4</sub><sup>-</sup>, removal of the sample matrix with sequential washes, before collection of the B in weak nitric acid.

Boron column chromatography has allowed for the successful measurement of B by MC-ICPMS, in turn leading to a rapid expansion of B isotope geochemistry. However, the column method has several drawbacks: hand-making columns leads to heterogeneities between them, hampering reproducibility; processing samples by columns can be time consuming, typically taking 8–12 hr to process 12–16 samples; and the open-topped nature of a

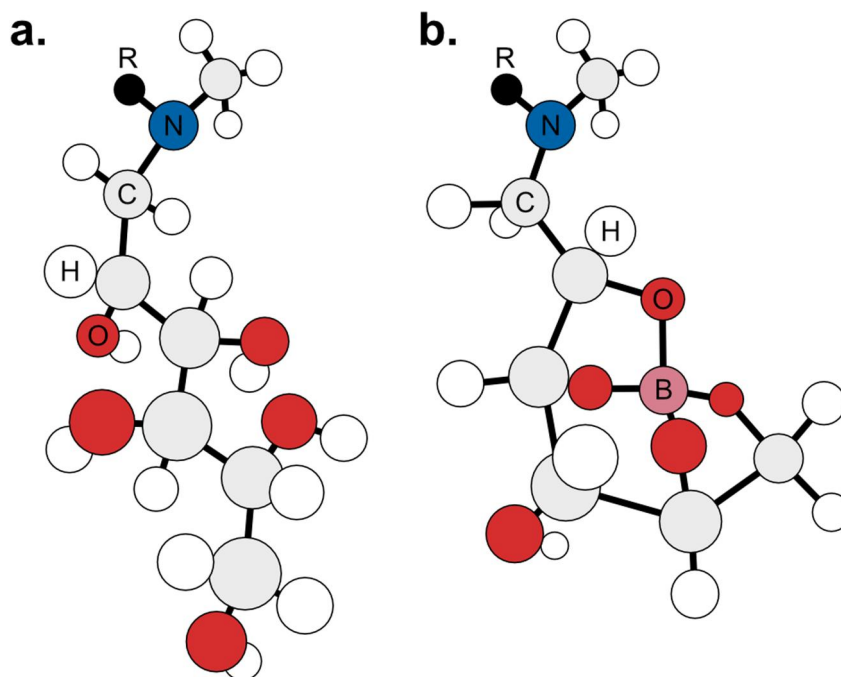


**Figure 1.** (a) Structure of the *N*-methylglucamine functional group in Amberlite IRA-743 resin. (b) Proposed tetradentate complex formed between Borate ion ( $B(OH)_4^-$ ) and the *N*-methylglucamine group in Amberlite IRA-743 resin. R = polystyrene chain (after Yoshimura et al., 1998).

column and long exposure time makes the method blank-sensitive, requiring exacting clean laboratory conditions and risking large blank correction on small samples (Kubota et al., 2021).

Here, we present a batch method for B separation using the same general purification chemistry, but in a centrifuge tube, allowing for greater control on the time of interaction between resin and solution, and with the potential for less airborne contamination due to its closed top. We test a wide array of controls on B purification using this method, identifying key operating parameters, and find some significant advantages, including faster throughput and lower procedural blank.

### 1.1. Resin Chemistry

Before discussing the batch method in detail, we briefly review aspects of amberlite resin chemistry given its central role in the chemical separation of B from its matrix. Amberlite resin is synthesized by animating a chloromethylated styrene-divinylbenzene copolymer (CSDC), itself an anion resin (Popat et al., 1988; Xiao et al., 2003), and is formed of a polystyrene backbone with an *N*-methylglucamine functional group. This group is able to bind with borate ions in a tetradentate complex (Figure 1b, Yoshimura et al., 1998) but does not bind with boric acid, allowing for the binding of B at high pH, removal of the sample matrix, and B collection at low pH as the bound borate ion is converted to boric acid.

Under the conditions that a typical dissolved and buffered carbonate sample is loaded onto the resin at (pH ~6), some B is complexed by calcium ( $CaH_2BO_3^+$ ), magnesium ( $MgH_2BO_3^+$ ) and sodium ( $NaH_2BO_3$ ). The concentration of these complexes increases with increasing pH (Figure 2c). However, this is a relatively minor component, and as free borate is drawn down and loaded onto the resin, the remainder will re-speciate.

## 2. Methods

Boron isotope measurements for this study were made by MC-ICPMS on the Neptune Plus in the St Andrews isotope Geochemistry laboratories (STAiG) at the University of St Andrews. Mass spectrometry procedures generally follow Foster (2008) and Rae et al. (2011), but with the addition of a small volume of concentrated HF to samples, standards and blanks to yield a solution of 0.3 M to aid washout (Misra et al., 2014; Zeebe &

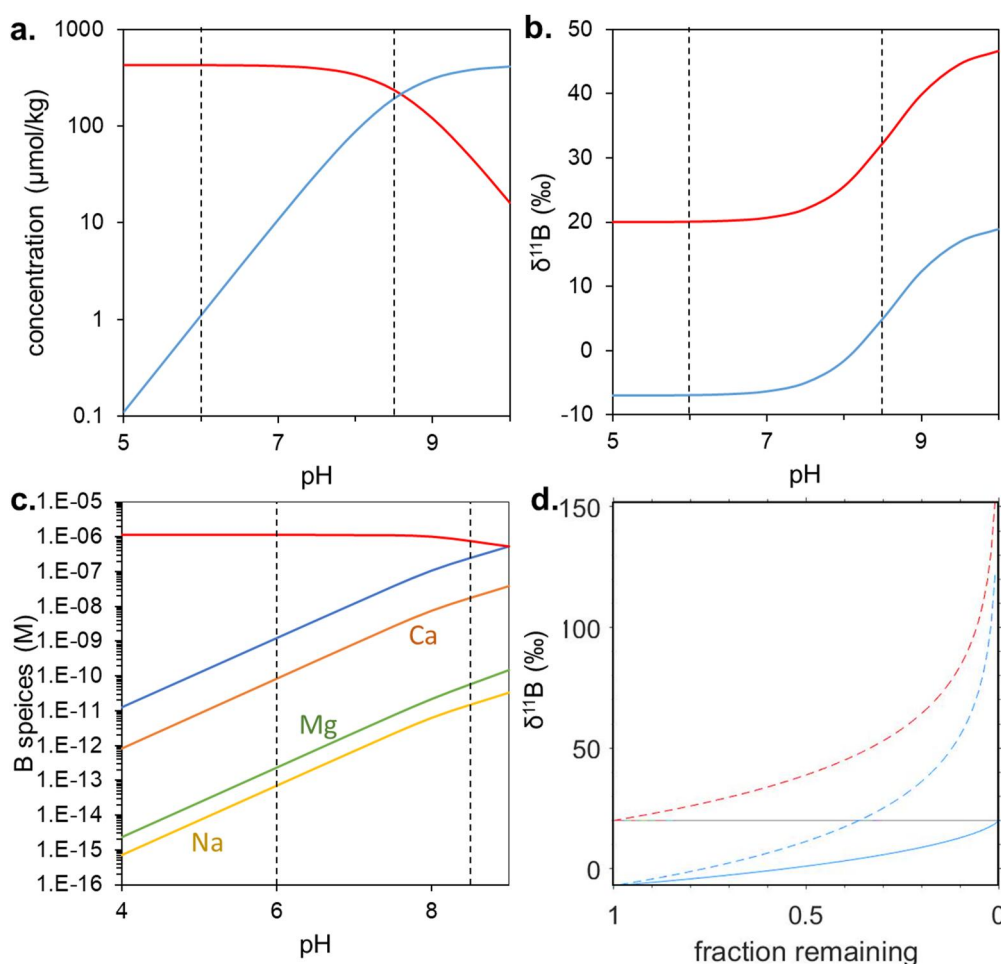


**Figure 2.** The impact of changing pH on B speciation and the isotopic composition of those species. (a) Speciation of boric acid ( $\text{B(OH)}_3$ , red) and borate ion ( $\text{B(OH)}_4^-$ , blue) at differing pH. (b)  $\delta^{11}\text{B}$  of boric acid and borate ion at differing pH with a total composition of 20‰. (c) Partitioning of boron into boric acid ( $\text{B(OH)}_3$ , red), borate ion ( $\text{B(OH)}_4^-$ , blue), and B complexed by calcium ( $\text{CaH}_2\text{BO}_3^+$ , orange), magnesium ( $\text{MgH}_2\text{BO}_3^+$ , green) and sodium ( $\text{NaH}_2\text{BO}_3$ , yellow), under conditions typical for a dissolved planktic foraminiferal sample that has been buffered for sample loading at differing pH, calculated in PHREEQC. (d)  $\delta^{11}\text{B}$  of boric acid and borate ion in solution (dashed red and blue lines, respectively) as borate ion is removed from the solution onto the resin during sample loading (solid blue line represents cumulative loaded borate) using a sample composition of 20‰. Black dashed lines indicate that the pH samples are loaded at (pH 6) and the pH resin is preconditioned to (pH 8.5).

Rae, 2020),  $10^{13} \Omega$  resistors to minimize the influence of thermal noise from the Faraday cup current amplifiers (Lloyd et al., 2018), and a low flow ( $\sim 35 \mu\text{l/min}$ ) self-aspirating nebulizer to enable sample analyses in triplicate. The reproducibility of this mass spectrometric method was assessed using boric acid standards analyzed as dummy samples that span the range of concentrations examined in this study (see Figure 3). Following Rae et al. (2011), we fit these data with an equation made up of two exponential terms, using exponents of  $-1$  and  $-0.5$  to represent the influences of amplifier noise and counting statistics, plus a constant representing inaccuracies in sample standard bracketing (or “flicker”; see John & Adkins, 2010). This fit is used to characterize the uncertainty arising from MC-ICPMS measurement on the analyses within this study. We note that this does not necessarily provide a full measure of reproducibility, which should include potential influences from sample purification and procedural blanks under typical operating conditions. However, as many of the tests presented here are designed to push the purification process to explore its limits, application of reproducibility based on typical operating conditions may in some cases be inappropriate, so we opt for this simple instrumental measure of uncertainty for consistency.

All sample purification and handling was carried out in a laminar flow hood within a class 100 clean lab equipped throughout with boron-free filters. All reagents used were of a high purity, using B-free water (MilliQ,  $18.2 \text{ M}\Omega\cdot\text{cm}$  at  $25^\circ\text{C}$ ), Teflon-distilled  $\text{HNO}_3$ , and super pure HF (ROMIL SpA). Ammonium acetate buffer was

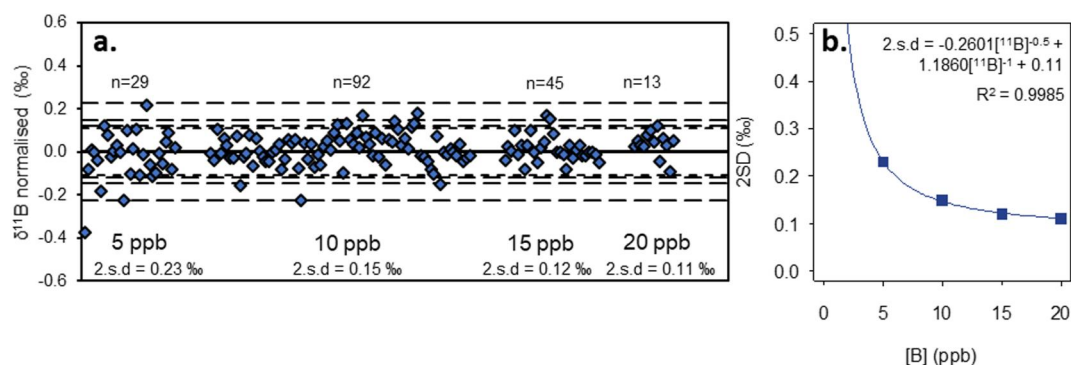


**Figure 3.** (a)  $\delta^{11}\text{B}$  offset of a boric acid standard measured (BIGD) relative to the long-term average (14.77‰) at different concentrations. (b) Reproducibility of BIGD at different concentrations and fit were used to characterize uncertainty.

made to yield 1.4 M ammonium hydroxide and 1.2 M acetic acid, before being cleaned by a batch method to remove B (see Supporting Information S1 for full details). Any carbonate standards and samples used were cleaned prior to dissolution using clay removal and oxidative cleaning steps described in Rae et al. (2011), developed from Barker et al. (2003), and dissolved in a combination of 100  $\mu\text{l}$  MilliQ and 20–300  $\mu\text{l}$   $\text{HNO}_3$ , with a small (~15%) split analyzed for trace elements on an Agilent 8900 ICP-QQQ. Some samples were purified for B using a regular gravity column procedure following Foster (2008) and a peri-pump column method (Xu et al., 2024) for comparison with our batch method.

To separate B from its matrix using the batch method, 1.5 ml centrifuge tubes are filled with 100  $\mu\text{l}$  precleaned Amberlite IRA-743 resin crushed and sieved to 63–125  $\mu\text{m}$  (for full details of resin preparation and cleaning see SI). All solutions are pipetted onto the resin, vortexed to ensure resin is in suspension, allowed to settle, and then centrifuged to ensure resin is at the bottom before pipetting off the supernatant (Figure 4). The resin is cleaned at the beginning of the procedure with  $3 \times 1\text{ ml}$  0.5 M  $\text{HNO}_3$  steps and  $2 \times 1\text{ ml}$  MilliQ steps. The resin is then preconditioned with 100  $\mu\text{l}$  of a pH 8.5 ammonium acetate buffer before the sample is loaded buffered to pH 6 at a ratio of 1.5:1 buffer:acid with an ammonium acetate buffer. The matrix is washed off with  $6 \times 500\text{ }\mu\text{l}$  MilliQ washes, before the B is collected in 500  $\mu\text{l}$  0.5 M  $\text{HNO}_3$ . Prior to storage, the resin is recleaned with  $3 \times 1\text{ ml}$  0.5 M  $\text{HNO}_3$  steps and  $2 \times 1\text{ ml}$  MilliQ steps, with brief vortexing at each step, and then stored in MilliQ. For a step by step procedure see the SI.

This method is capable of producing data with  $<0.2\%$  2SD reproducibility. However, to achieve this, it is critical to operate within a certain parameter space. The batch method developed here works for a range of sample ionic strengths, volumes and concentrations. In the following sections, we detail the key sensitivity tests which determined these viable parameter spaces. The majority of these tests use NIST RM 8301 foram (8301f), which has a B/Ca of  $\sim 140\text{ }\mu\text{mol/mol}$  and minor and trace element composition similar to foraminiferal carbonate. 8301f has presented analytical challenges in previous studies (see discussion in Stewart et al., 2021), making it a good

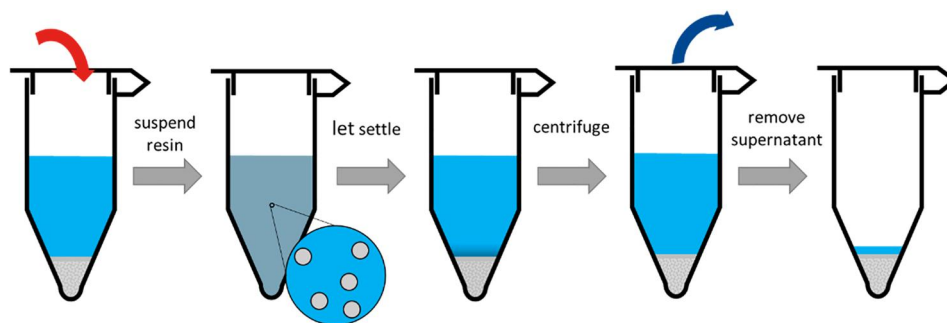


**Figure 4.** Schematic overview of batch procedure. Solutions are added to 100  $\mu\text{l}$  of Amberlite IRA-743 resin in a 1.5 ml centrifuge tube, which is then vortexed to suspend the resin in the solution, allowed to mostly settle ( $\sim 1\text{ min}$  for a  $<200\text{ }\mu\text{l}$  solution, 2–3 min for a  $>200\text{ }\mu\text{l}$  solution), centrifuged for 60 s at 13,000 rpm to ensure all resin is at the bottom and the supernatant removed to allow the next solution to be pipetted in.

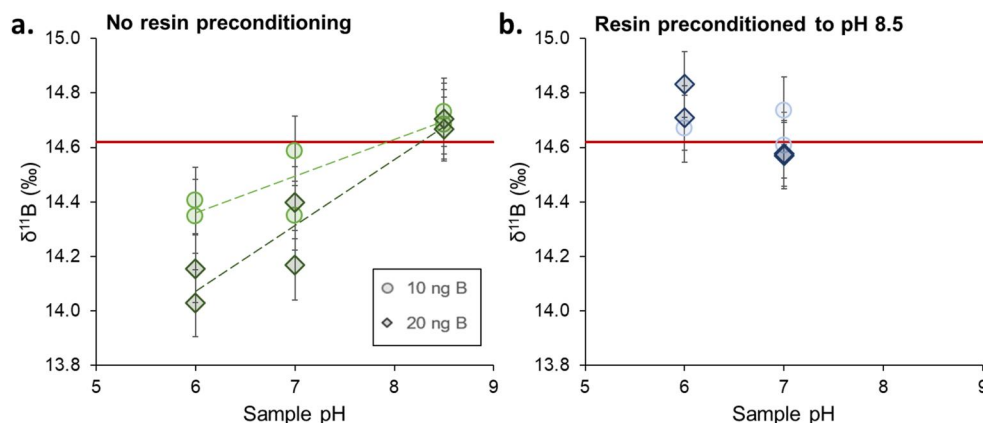


**Figure 5.** NIST 8301f loaded at a range of pHs and sizes (mass of B indicated in key) both without (a) and with (b) preconditioning with a pH 8.5 buffer. Raising the pH a sample is loaded at (a) combats the negative offset seen in the batch method compared to columns and published standard values. The same effect can be seen when preconditioning a pH 8.5 buffer and loading the sample buffered to pH 6 (b). Dark red line is no offset from long-term average  $\delta^{11}\text{B}$  (14.62‰), error bars are 2SD based on machine uncertainty (see methods).

test for the robustness of an analytical method. In addition, we test several other carbonate standards, seawater, and a wide variety of foraminiferal samples, which were split and also analyzed following the well-established column-based procedure.

### 3. Key Sensitivity Tests

#### 3.1. Sample Load and Preconditioning pH

To optimize the binding of B to the resin, we experimented with different pH conditions during sample loading. Amberlite IRA-743 resin has a high affinity for borate and loads B most effectively at high pH, where more B is present as borate. The amino group present in the Amberlite IRA-743 structure (Figure 1) raises the pH of the resin relative to the solution, which results in the highest affinity for B at a  $\text{pH}_{\text{resin}}$  of 9, which is equivalent to a  $\text{pH}_{\text{resin}}$  11.5 (Yoshimura et al., 1998). However, loading dissolved carbonate samples at pH 9 is unfavorable, as there is a risk of carbonate precipitate formation, which is a potential source of  $\delta^{11}\text{B}$  fractionation and B loss. Additionally, there is the potential for the formation of ion hydroxides (i.e.,  $\text{Ca}(\text{OH})_2$ ,  $\text{Mg}(\text{OH})_2$ ,  $\text{Fe}(\text{OH})_2$ ) from the dissolved sample, which are subsequently retained by the resin, inhibiting B binding (Aggarwal & Palmer, 1995). For this reason, column procedures have typically buffered samples to pH ~6 prior to loading (Foster, 2008), high enough to notably increase the borate proportion and the resin's affinity for B, but low enough to avoid precipitate formation.

When a sample is loaded at a pH comparable to columns (pH 6–7), we observe a negative offset  $\delta^{11}\text{B}$  in standards purified using the batch procedure, which is seen more strongly for larger samples (Figure 5a), and indicates incomplete loading (Figure 2d). Raising the load pH to 8.5 in the batch method combats this negative offset (Figure 5a), though is not our preferred solution due to the precipitation risks mentioned above. The same effect can be attained instead by preconditioning the resin with a pH 8.5 buffer prior to sample loading, removing this solution, and then loading the sample buffered to pH 6 (Figure 5b). We tested a range of pH for the pre-load buffer to test for any influence (e.g., due to residual high pH pre-load buffer causing precipitate formation) and found no trend in  $\delta^{11}\text{B}$  for the pH range tested (6–9) for large benthic (*C. wuellerstorfi*) and planktic (*O. universa*) foraminiferal samples (Figure S1 in Supporting Information S1), suggesting no influence from

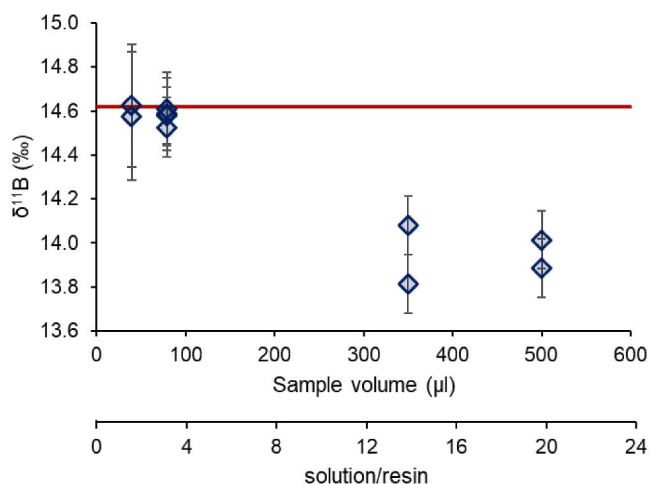


**Figure 6.** Influence of sample volume on  $\delta^{11}\text{B}$  for NIST 8301f using 25  $\mu\text{l}$  resin volume. Solution volume to resin volume ratio is shown underneath as a secondary axis. NIST 8301f at several concentrations (for details see Supporting Information S2) was diluted with additional 0.5 M  $\text{HNO}_3$ , ammonium acetate buffer and MilliQ in a ratio roughly proportional to a typical foraminiferal sample (1:1:2 acid:MilliQ:buffer). Loading large total sample volumes negatively fractionates the measured  $\delta^{11}\text{B}$ . Dark red line is no offset from long-term average  $\delta^{11}\text{B}$  (14.62‰), error bars are 2SD based on machine uncertainty (see methods).

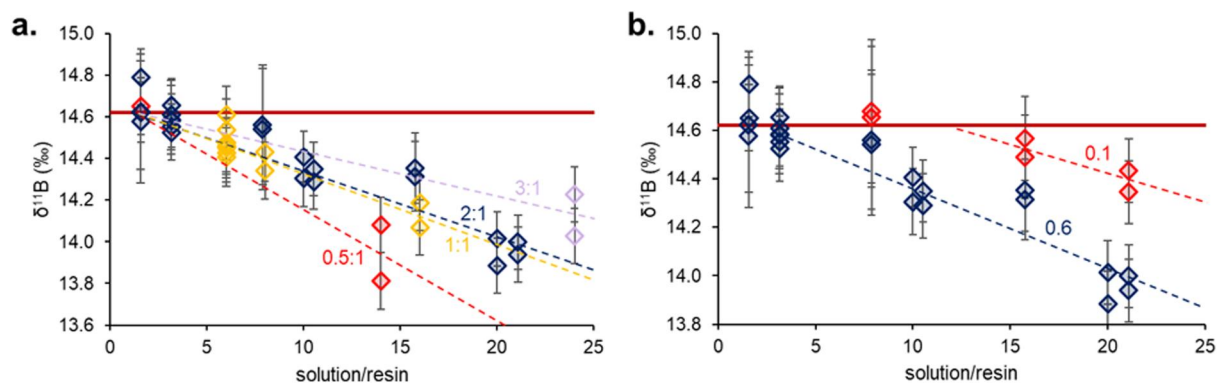


**Figure 7.** The effect of changing the volume ratio of the sample solution relative to the resin on sample loading, as a function of (a) buffer/acid ratio and (b) ionic strength. Dark red line is no offset from long-term average  $\delta^{11}\text{B}$  (14.62‰), error bars are 2SD based on machine uncertainty (see methods). In all cases sample loading is facilitated by a lower solution to resin volume ratio; negative  $\delta^{11}\text{B}$  offsets, indicating incomplete sample loading, are observed as the relative solution volume rises. The nature of this relationship is also modulated by buffer to acid ratio (symbols and labeled lines in (a)) and by ionic strength (symbols and labeled lines in (b)), with ionic strength given here as the volume of acid and buffer divided by the total sample volume. Sample loading is facilitated by higher buffer/acid ratios, allowing the same volume of solution to be loaded with a smaller volume of resin, and in samples with lower ionic strength. The buffer/acid ratio was held constant at 2:1 for the experiments in (b).

carbonate or hydroxide precipitation across this preconditioning pH range and for the types of samples measured here.

### 3.2. Sample Volume, Buffer to Acid Ratio, and Ionic Strength

Boron content can vary significantly in samples analyzed for  $\delta^{11}\text{B}$ , leading to a range of sample volumes to attain a given mass of boron for analysis. While using the same resin volume as a column (25  $\mu\text{l}$ , Foster, 2008) yielded excellent results for small volumes of standards with relatively high B concentrations (Figure 6), it did not perform as well for more diluted, larger volume samples, which are more representative of a typical foraminiferal sample. In these cases the measured  $\delta^{11}\text{B}$  is negatively offset relative to published values (Figure 6), again suggesting some loss of B due to incomplete loading.

This sample volume offset can be combatted by increasing resin volume, provided the volume of preconditioning buffer is scaled accordingly to ensure the full resin volume pH is sufficiently elevated. However, the relationship

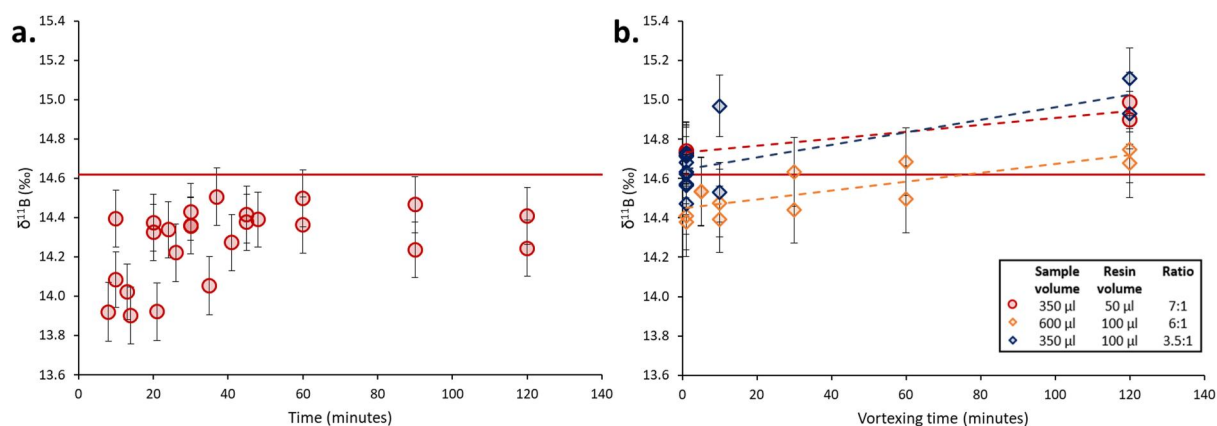


**Figure 8.** Influence of loading time on large volume samples. Mixing of solution and resin was tested by either (a) vortexing briefly (~3–5 s) every 5 min or (b) constantly for periods of 1–140 min for a range of sample and resin volumes. Symbols represent the different sample and resin volumes: red circles 350  $\mu\text{l}$  sample volume 50  $\mu\text{l}$  resin volume, orange diamonds 600  $\mu\text{l}$  sample volume 100  $\mu\text{l}$  resin volume, blue diamonds 350  $\mu\text{l}$  sample volume 100  $\mu\text{l}$  resin volume. Dark red line is no offset from long-term average  $\delta^{11}\text{B}$  (14.62‰), error bars are 2SD based on instrumental uncertainty (see methods). Data in (a) are negatively offset due to incomplete loading, a result of their high solution to resin ratio. Increasing the interaction time between resin and solution by increasing the mixing time helps partially decrease this offset, but increasing mixing time is not able to fully compensate for too low a solution to resin ratio. Continuous vortexing (b) rapidly achieves full mixing and equilibration for samples with a low, optimized solution to resin ratio, but overly extensive continuous vortexing can lead to loss of light boron and positively offset  $\delta^{11}\text{B}$ . Our optimized method uses 1 min of continuous vortexing.

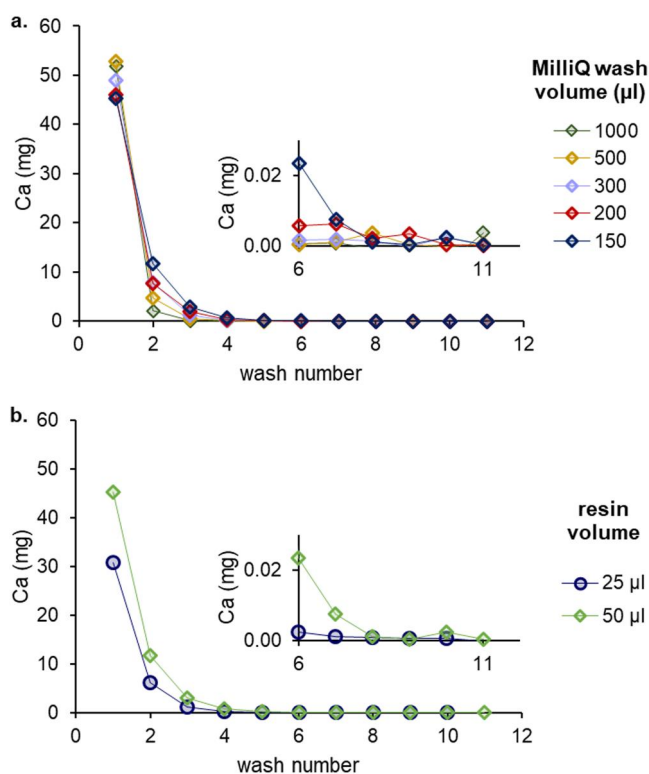


**Figure 9.** Ca (mg) in Milli-Q washes. (a) At different wash volumes (in  $\mu\text{l}$ ) and (b) For different resin volumes with the same wash volume (150  $\mu\text{l}$ ). Note that a significant proportion of the Ca is removed when the load is removed (not shown here), which will be greater the smaller the resin volume.

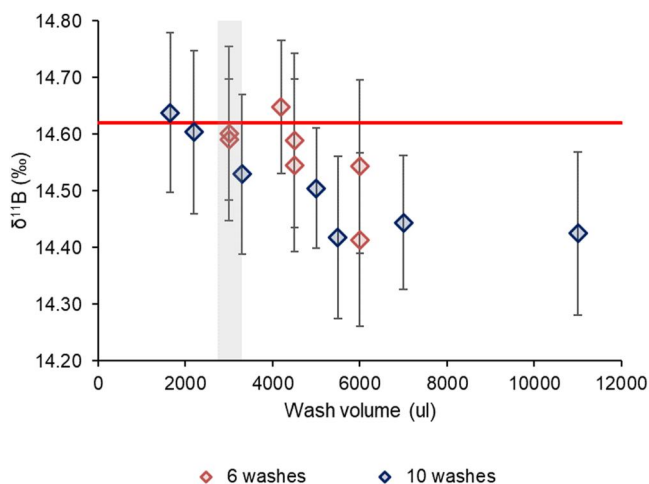


**Figure 10.**  $\delta^{11}\text{B}$  with increased total Milli-Q wash volume using 100  $\mu\text{l}$  resin volume. When larger total wash volumes are used,  $\delta^{11}\text{B}$  is offset negatively from the long-term average (14.62‰). For equivalent total wash volumes, this offset tends to be larger for a greater total number of washes. Note that the typical procedure uses a total wash volume of 3,000  $\mu\text{l}$  (6  $\times$  500  $\mu\text{l}$ , indicated by gray bar). Dark red line is no offset from long-term average  $\delta^{11}\text{B}$  (14.62‰), error bars are 2SD based on machine uncertainty (see methods).

between sample volume, resin volume and the  $\delta^{11}\text{B}$  offset between measured and published values for NIST 8301f can also be influenced by other factors. In the column procedure, samples are typically buffered to pH 6 by the addition of a 1.4 M ammonium hydroxide and 1.2 M acetic acid buffer, with 2 volumes of buffer added per volume of 0.5 M  $\text{HNO}_3$  that was used in sample dissolution (Foster, 2008). However, we found that changing this buffer/acid ratio for the batch method changes the gradient of the sample/resin ratio versus  $\delta^{11}\text{B}$  offset relationship (Figure 7a). Lower buffer to acid ratios lead to increased gradients between sample/resin volume and  $\delta^{11}\text{B}$  offset, so for the same volumes of solution and resin, a greater offset will be seen. In other words, complete loading is enabled by the combination of high resin to sample volumes, promoting interaction between active sites on the resin and borate ions, and high buffer to acid volumes, leading to higher pH and greater abundance of borate. However, there are drawbacks of both excessive resin and buffer volumes. As detailed in Section 3.5, increasing the resin volume requires an increase in the elution volume, resulting in dilution of B in the solutions used for analysis (as the volatile nature of B precludes concentration by sample dry-down). The ionic strength (here proxied by the volume of acid and buffer divided by the total volume of the sample) also has an effect on the relationship between sample volume, resin volume and the  $\delta^{11}\text{B}$  offset, where a sample with a lower ionic strength requires less resin to achieve full loading than a sample with a higher ionic strength (Figure 7b). This is similar to the results of Lemarchand et al. (2002), who showed that high ionic strength inhibits the fixation of B onto the resin.

To address these issues, we increased the resin volume in the batch method from 25 to 100  $\mu\text{l}$ , scaling the volume of the pH 8.5 buffer used to precondition the resin to 100  $\mu\text{l}$  accordingly, and used a 1.5:1 ratio of buffer to dissolution acid. This allows a sample of up to 350  $\mu\text{l}$  total volume (e.g., consisting of 100  $\mu\text{l}$  MilliQ, 100  $\mu\text{l}$  0.5 M  $\text{HNO}_3$  and 150  $\mu\text{l}$  pH 6 ammonium acetate buffer) to load to completion. Increasing the resin volume to 100  $\mu\text{l}$  requires an increase in the elution volume to 500  $\mu\text{l}$  0.5 M  $\text{HNO}_3$  (see Section 3.5), as the elution volume required is roughly proportional to the resin volume. For samples above this total volume, a larger resin volume is likely necessary. Alternatively, a large volume sample may be split between two batch tubes, ensuring that the volume loaded onto each individual batch tube remains below 350  $\mu\text{l}$ , and the B from both batch tubes was collected in the same eluant—eluting one with 500  $\mu\text{l}$  0.5 M  $\text{HNO}_3$ , then taking that same acid to elute the second.

### 3.3. Loading Time

Load efficiency can, to an extent, be influenced by the time for interaction between the resin and sample during sample loading. We explored a range of loading times assisted by a vortexor to ensure thorough mixing and interaction between solution and resin, either vortexing continuously or vortexing briefly ( $\sim 3\text{--}5$  s) until the resin was in suspension every 5 min. Note that some of these tests were carried out at higher than optimal ratios of sample solution to resin volume (see Section 3.2), which reduces the efficiency of sample-resin interaction, and thus provides a harder test for loading optimization. A trend is seen with increasing loading/vortexing time with both techniques. For the high sample volume to resin volume tests in Figure 8a,  $\delta^{11}\text{B}$  data are offset light due to incomplete loading (see also Figure 7), but the size of this offset is reduced by repeated mixings every 5 min. Complete loading can be efficiently achieved with continuous mixing, with accurate values attained

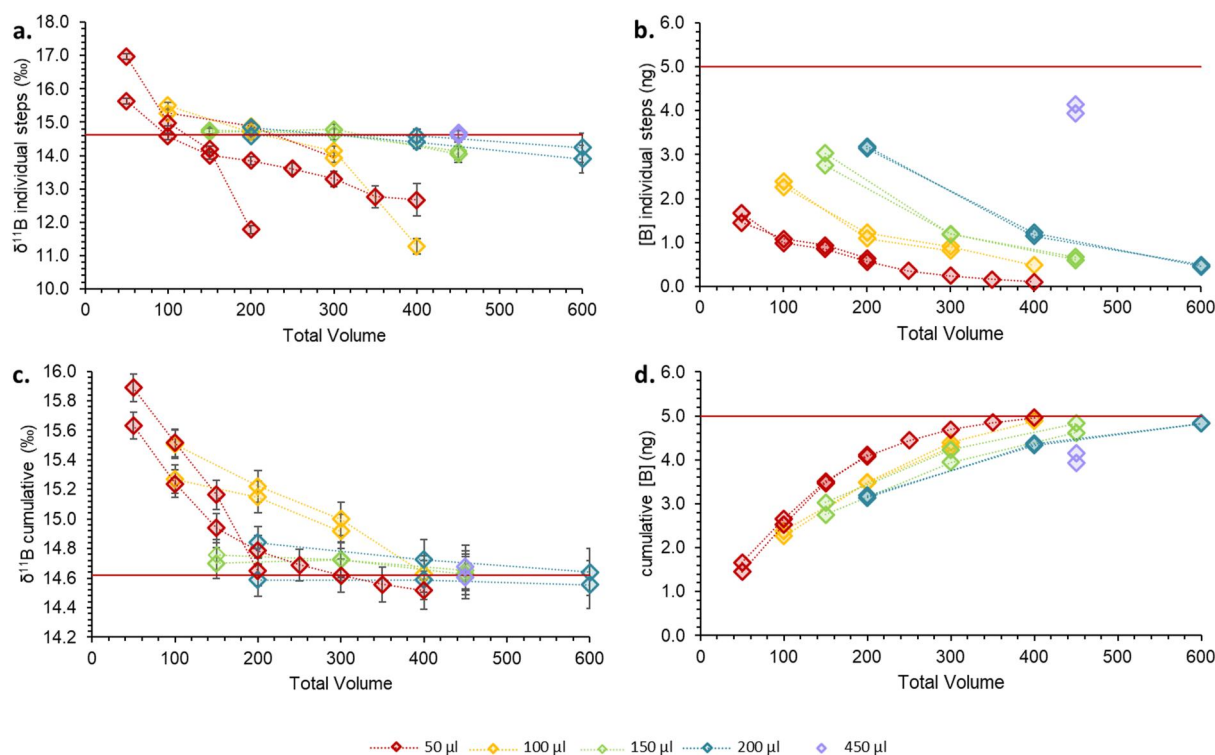


**Figure 11.** Impact of elution volume on  $\delta^{11}\text{B}$ . All tests use a 50  $\mu\text{l}$  resin volume. Different symbol colors refer to the volume of individual elution steps. (a)  $\delta^{11}\text{B}$  of each elution fraction; initial B eluted is isotopically heavy, and the last B to be eluted is isotopically light. (b) [B] eluted in each elution fraction. c. Cumulative  $\delta^{11}\text{B}$  with elution volume; the first B to be eluted is isotopically heavy but reaches the long-term average  $\delta^{11}\text{B}$  (14.62‰) after 450  $\mu\text{l}$  0.5 M  $\text{HNO}_3$ . d. Cumulative [B] eluted with increasing elution volume. The dark red line in panels (a and c) is no offset from the long-term average  $\delta^{11}\text{B}$  (14.62‰), error bars are 2SD based on machine uncertainty (see methods). The red line in panels (b and d) indicates the concentration loaded.

within 1 min provided the solution to resin volume is optimized (Figure 8b). We note however that continuous vortexing for more extended periods results in a slight increase in  $\delta^{11}\text{B}$ , eventually leading to values heavier than the long-term averages and the published value for NIST 8301f (Figure 8, Stewart et al., 2021). This indicates that excessive vortexing may lead to loss of light B driving the measured  $\delta^{11}\text{B}$  isotopically heavy. One potential explanation could be that the increased shaking time promotes the evaporation of boric acid via microdroplet formation and heating, with preferential loss of lighter  $^{10}\text{B}$  boric acid. Hence samples are loaded for 1 min of constant vortexing, which minimizes the chance of volatile boron loss and achieves complete sample loading provided the solution/resin ratio is optimized.

### 3.4. Washes

In order to remove the calcium carbonate matrix from the sample, a series of Milli-Q washes is used after the B is loaded onto the resin. For columns, these washes are directed around the column's interior in order to rinse down the sides, and the time the process takes is determined by the flow rate of the column and the total number and volume of washes. For the batch, a small volume wash will take roughly the same time as a large volume wash, and the time the process takes is determined by the number of times a solution is pipetted on and off the resin. Hence, a smaller number of larger volume washes are advantageous to the batch compared to columns. The Ca content of the washes shows the extent of matrix removal and was used to determine that  $6 \times 500 \mu\text{l}$  Milli-Q washes remove the matrix as effectively as  $11 \times 150 \mu\text{l}$  washes (Figure 9). It should be noted that for a smaller resin volume, a smaller number of washes can be used (Figure 9b), and that with a very large total wash volume, B begins to be washed off the resin too, leading to negatively offset  $\delta^{11}\text{B}$  (Figure 10) as the initial B loss from the resin is isotopically heavy. Additionally, the total number of washes and the volume of washes is not a direct 1:1 relationship thus  $11 \times 150 \mu\text{l}$  washes will remove the matrix equivalently to  $10 \times 200 \mu\text{l}$  washes,  $9 \times 300 \mu\text{l}$  washes,  $6 \times 500 \mu\text{l}$  washes or  $5 \times 1 \text{ ml}$  washes.



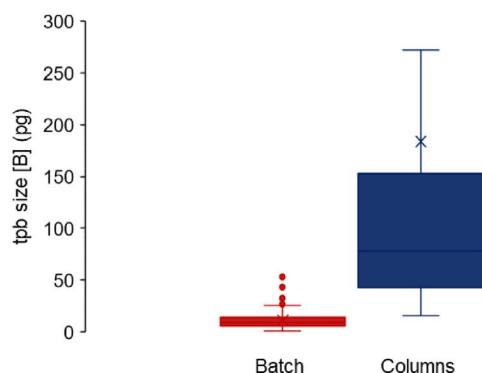


**Figure 12.** Comparison of Total procedural blank (TPB) size through the batch method ( $n = 262$ ) and columns ( $n = 103$ ) between January 2019 and May 2021 in the STAiG lab. Batch TPBs are lower and have a more consistent size than column TPBs, though some of the larger column blanks were likely driven by problems with resin contamination.

### 3.5. Elution Time and Volume

During elution, the pH of the solution and resin is lowered by the addition of 0.5 M  $\text{HNO}_3$ . This converts the B on the resin from  $\text{B}(\text{OH})_4^-$  to  $\text{B}(\text{OH})_3$ . If this reaction is not taken to completion, the measured  $\delta^{11}\text{B}$  will be fractionated isotopically heavy due to some  $\text{B}(\text{OH})_4^-$  (which is isotopically relatively light) remaining adhered to the resin (Figures 2 and 11). During column chromatography, elution is achieved by a series of sequential  $\text{HNO}_3$  steps to ensure that eluted B is efficiently transported through the column volume for collection. In contrast, for the batch method, eluting in a single step achieves the same result and is more time efficient. Eluting the resin sequentially in 50, 100, 150, 200, and 450  $\mu\text{l}$  steps shows that the first B collected is isotopically heavy and the final B released is isotopically light (Figure 11). The volume of elution acid required to take this reaction to completion is likely related to the resin volume: 50  $\mu\text{l}$  resin can be eluted in 450  $\mu\text{l}$  (and likely in smaller volumes, though as this is the minimum volume for our triple-replicate MC-ICPMS method, we have not explored these smaller elution volumes in detail); our finalized procedure with 100  $\mu\text{l}$  resin uses 500  $\mu\text{l}$  of elution acid

( $5 \times$  the resin volume). Eluting in one step is preferable both for time efficiency and because it means any residual boron (e.g., in the resin pore space) is not isotopically different from the B collected. This has the additional benefit of making the procedure more robust to user differences, as it reduces any sensitivity to the amount of solution left behind on top of the resin and in the pore space.

Elution is a quick process. We tested this by vortexing samples every 5 min for up to 45 min and found no trend between  $\delta^{11}\text{B}$  and time interacted with eluting acid (Figure S2 in Supporting Information S1). In the current procedure, resin is vortexed until it is suspended in the eluant and then centrifuged.

### 3.6. Additional Tests

The steps described above give the key parameters for this procedure. However in developing the method we also tested a range of additional factors, which we report below.

#### 3.6.1. High pH Cleaning Step

Total procedural blanks (TPBs) through the batch method are low and consistent. In the same time period at St Andrews, TPBs were typically below 20 pg through the batch method compared to values  $\sim 20$ –200 pg through columns, though some of these higher column tpbs may have been driven by anomalous resin contamination problems (Figure 12). We found that batch TPBs may further be reduced using a high pH cleaning step at the start of the procedure prior to the resin cleaning stage. Earlier work suggested that at a solution pH of 10, any B species

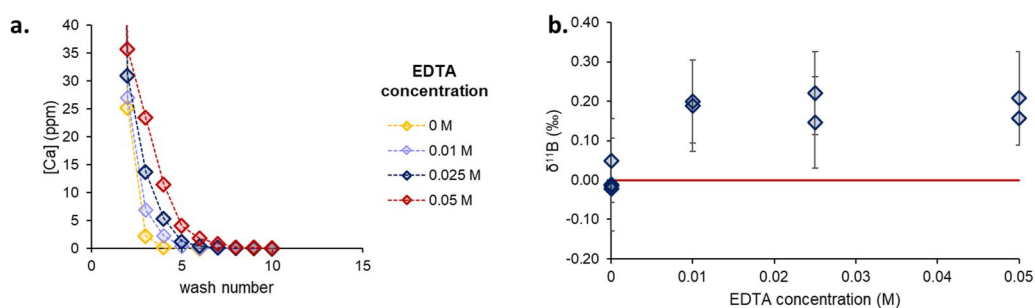


**Figure 13.** Impact of adding EDTA to the sample loading stage at different concentrations on matrix removal (a) and measured  $\delta^{11}\text{B}$  (b). (a)  $[\text{Ca}]$  in MilliQ washes for different concentrations of EDTA. All washes with 500  $\mu\text{l}$  MilliQ. b.  $\delta^{11}\text{B}$  for NIST 8301f were measured with different concentrations of EDTA. To achieve full matrix removal with these volumes of EDTA, a total wash volume of 5,000  $\mu\text{l}$  was used (10  $\times$  500  $\mu\text{l}$  washes), including for the 0 EDTA sample. This results in an isotopically light offset, so standards here normalized to the 8301f run with 0M EDTA (dark red line). Addition of EDTA then adds a second positive offset. All concentrations of EDTA show a positive offset compared to standards run without EDTA. Error bars are 2SD based on machine uncertainty (see methods).

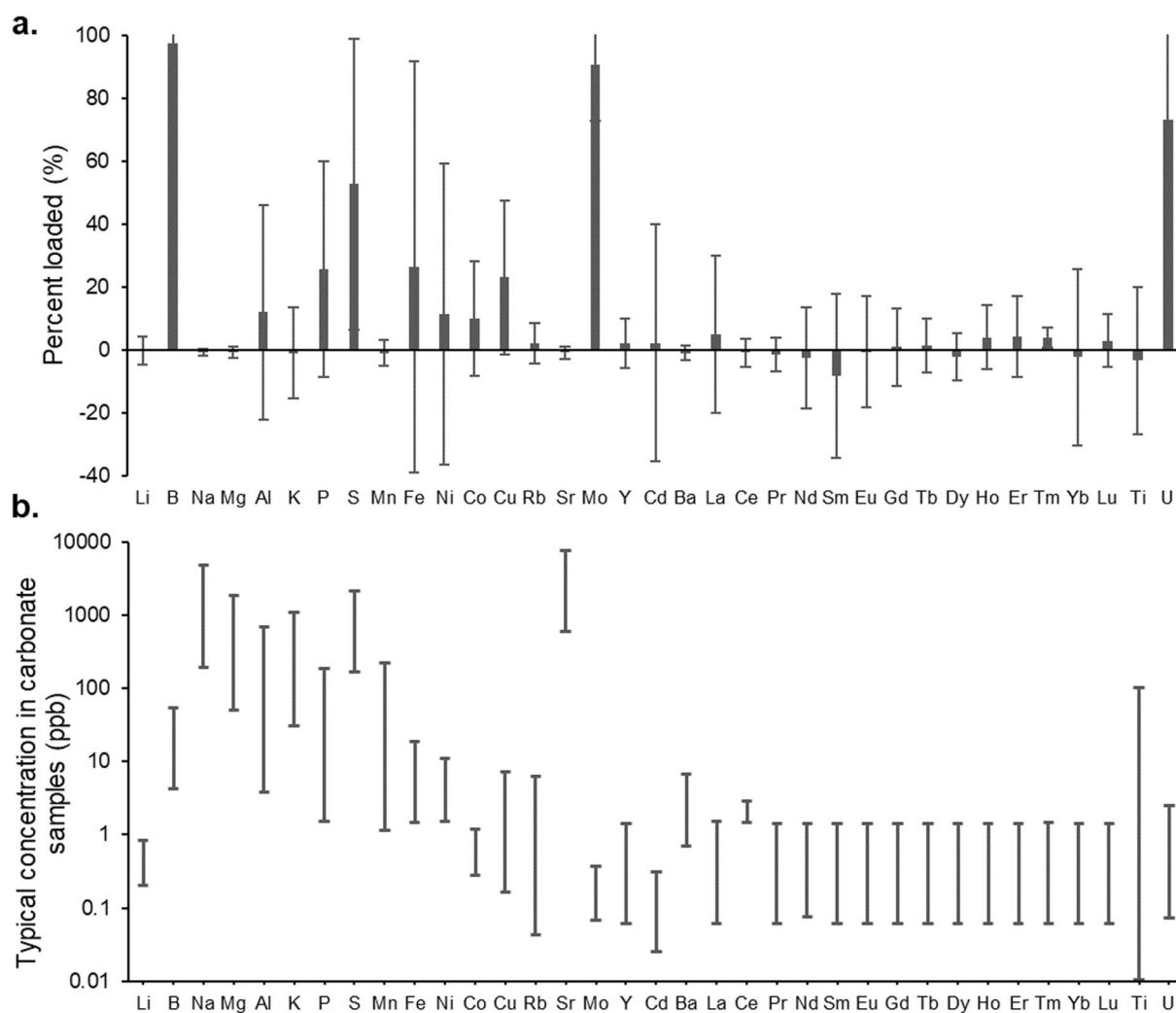


**Figure 14.** Potential interaction of other elements with Amberlite IRA-743 resin. (a) Trace elements were measured before and after sample loading (with the after value measured in the removed sample) for four standards with a range of compositions. Figure shows the percentage difference between these measurements, representing the proportion of each element loaded onto resin (and/or sticking to the tube). Bars are averages for all standards and error bars show  $\pm 2SD$ . (b) Range of elemental concentrations in synthetic standards tested, which represent a wide range of carbonates (foraminifera, coccolithophores, corals and limestones).

**Table 1**

Summary of Example Resins, Preconditioning Buffers, Samples, and Elution Volumes

Resin volume ( $\mu\text{l}$ )		25	50	100
Preconditioning buffer volume ( $\mu\text{l}$ )		25	50	100
Max sample volume ( $\mu\text{l}$ )	Total	82.5	175	350
	MilliQ	25	50	100
	0.5 M $\text{HNO}_3$	25	50	100
	Buffer	32.5	75	150
Minimum elution volume ( $\mu\text{l}$ )		<450	<450	500

Note. Acid volume is the 0.5 M  $\text{HNO}_3$  used for carbonate sample dissolution. MilliQ is also used during sample dissolution to avoid leaching residual silicate material. Buffer volume is calculated at a buffer:acid volume ratio of 1.5:1.

interacting with the resin is converted to borate ion with the presence of B as boric acid being very unlikely (Aggarwal & Palmer, 1995; Xiao et al., 2003). This may be leveraged to remove recalcitrant B bound to the resin in other forms, which may slowly leach off and lead to increased TPBs. To test this, we added ultrapure ammonium hydroxide ( $\text{NH}_4\text{OH}$ ) to B-free MilliQ until it reached a pH of 10. This pH elevated MilliQ was included as a high pH cleaning step prior to the resin-cleaning stage. We then carried out the full batch procedure, including resin-cleaning, “loading” (in this case of an acid-MQ-buffer dummy sample), matrix removal, and elution. TPBs from batch tubes receiving this treatment were on average  $\sim 2.5$  times lower than those which did not (5 pg B with a high pH wash compared to 13 pg B without). This suggests that there may be a small amount of recalcitrant B bound to the resin, perhaps not as borate ions. The addition of a high pH cleaning step, which converts any residual boron to borate ion, allows B to be more effectively washed off the resin during subsequent acid washes. As blanks are typically low for the batch method this is not part of our routine procedure but

**Table 2**  
*Long-Term Averages and Variability for Boric Acids, and Synthetic and Natural Carbonate Standards Measured at the University of St Andrews, Compared to Published Values*

	Standard	B/Ca μmol/mol	Our long term			Published			Reference
			Average	2SD	n	Average	2SD	n	
Boric acids (non-purified)	AE121	n/a	19.63	0.15	504	19.9	0.6	22	Vogl and Rosner (2012)
	BIGD	n/a	14.77	0.19	209	19.71	0.07	39	Stewart et al. (2021)
Synthetic carbonates	NIST 8301f	139	14.62	0.21	218	14.51	0.17	82	Stewart et al. (2021)
	NIST 8301c	528	24.25	0.21	31	24.17	0.17	83	Stewart et al. (2021)
Natural carbonates	JCP-1	460	24.40	0.36	9	24.25	0.22	103	Gutjahr et al. (2020)
	JCT-1	191	16.26	0.16	10	16.24	0.38	108	Gutjahr et al. (2020)
	STG-F1	59	16.29	0.21	11	16.25	0.26	8	Xu et al. (2024)

*Note.* Boric acid values listed have not undergone purification, so don't provide a test of the batch method, but are included to help illustrate measurement accuracy. Studies providing reference  $\delta^{11}\text{B}$  values are listed; JCP-1 and JCT-1B/Ca ratios are taken from Hathorne et al. (2013). These average and standard deviation values are made up of analyses of different sample sizes, so don't necessarily reflect the optimal uncertainties achievable at larger sample size—see Figure 15. Published 2SD for synthetic and natural carbonates represent the 2SD on the averages from labs in the interlaboratory comparison, rather than 2SD on the individual measurements.

may prove useful when measuring small samples where procedural blank correction contributes a large part of the uncertainty.

### 3.6.2. Ca-Complexing Agents

Some groups use a cation column, prior to B purification with an Amberlite IRA-743 column, in order to remove some of the major cations from the sample prior to loading (Lemarchand et al., 2002; McCulloch et al., 2014). This reduces the chances of  $\text{CaCO}_3$  precipitation/ion hydroxide formation and/or the interaction between cations and the resin. As an alternative, we tested the addition of various Ca-complexing agents to the buffer during loading (EDTA, citric acid, BAPTA) to reduce the activity of  $\text{Ca}^{2+}$ —the major ion in the dissolved carbonate solution—and thus its potential for interaction with B or the resin. Complexing agents were added to the buffer for these tests, with the solutions made up using the same ammonium hydroxide concentration and pH as the typical buffer, and having the complexing agents replace some of the acetic acid. We found that the presence of these complexing agents required a larger number of washes to sufficiently remove the matrix (Figure 13a). This large number of washes is impractical as it starts to wash off B (Figure 10), fractionating the sample isotopically light. For EDTA and citric acid we also found standards were offset heavy relative to standards run with our typical

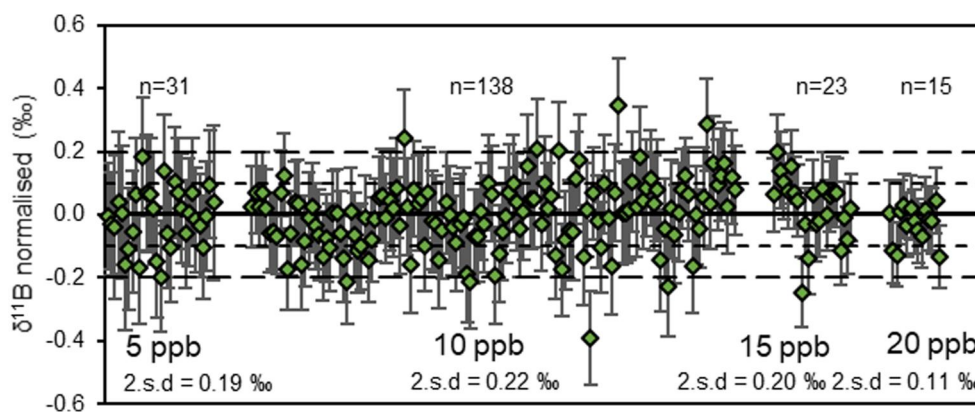


**Figure 15.**  $\delta^{11}\text{B}$  offset of a synthetic standard (NIST 8301f), which has been through chemistry relative to the long term average at different concentrations (14.62‰). Error bars are 2SD based on machine uncertainty (see methods). Dashed lines represent  $\pm 0.1$  and  $0.2‰$ .

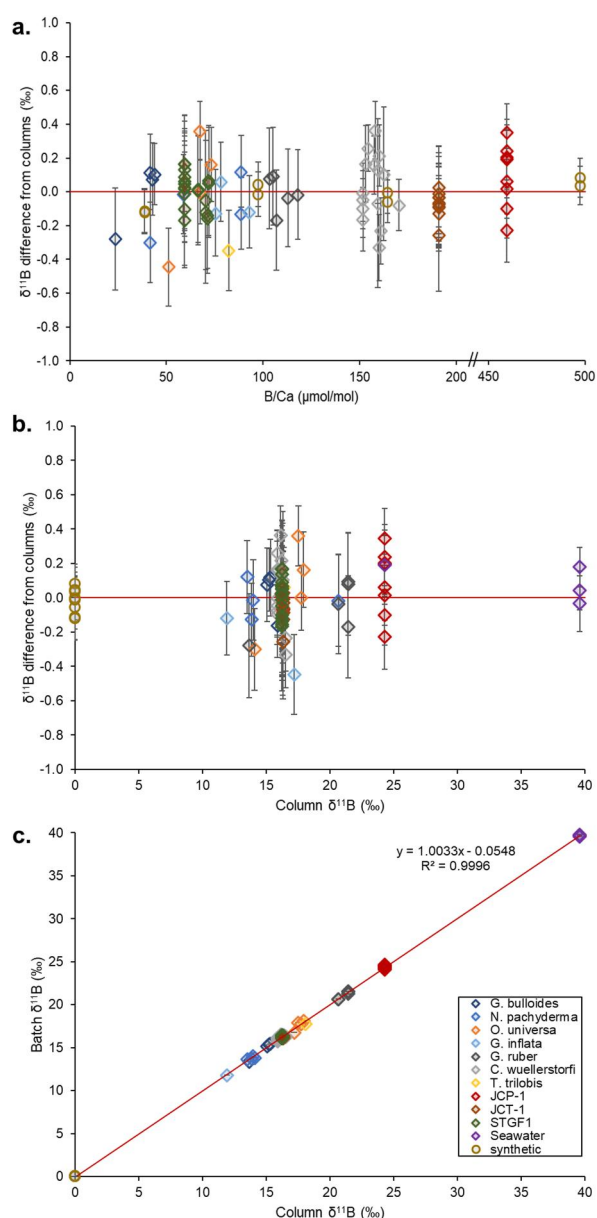


**Figure 16.** Measured  $\delta^{11}\text{B}$  after B separation by the batch method compared with measured  $\delta^{11}\text{B}$  through columns for a range of natural and synthetic carbonates. (a) Difference between  $\delta^{11}\text{B}$  measured by batch and columns plotted against sample B/Ca for a range of natural and synthetic standards. Synthetic standards are doped with NIST 951 to give a known  $\delta^{11}\text{B}$  with a variety of matrix compositions. Natural carbonates are measured where possible with columns and the batch method on the same dissolved solution (for details see Supporting Information S2). (b) Difference between  $\delta^{11}\text{B}$  measured by batch and columns plotted against measured column  $\delta^{11}\text{B}$  value. (c) Cross plot of  $\delta^{11}\text{B}$  measured using the batch and column methods. Column values are from this study and Gutjahr et al. (2020). Dark red line is no offset from column  $\delta^{11}\text{B}$ , error bars are 2SD based on instrumental uncertainty for batch  $\delta^{11}\text{B}$  and column values measured on the same solution as part of this study (see methods). When comparing to an average column value for a standard or sample, uncertainty for the column value is the 2SD on replicates of that sample (see Supporting Information S2 for details).

ammonium acetate buffer (Figure 13b), likely due to some interaction between the complexing agent and B. Given these drawbacks, and as no benefits were seen in the types of samples tested here, Ca-complexing agents are not included in the final procedure.

### 3.6.3. Binding of Other Elements to Amberlite IRA-743 Resin

The potential for other elements to bind to the resin and hence compete with B binding, or to release during elution and drive a matrix effect during measurement could potentially lead to reproducibility issues. We tested this by loading 4 synthetic carbonate standards with a range of compositions (Figure 14b) and measuring their trace and rare earth element composition before and after loading. While Amberlite IRA-743 resin is B specific, other elements also bind to the resin during loading, most notably Mo and U, though also some P, S, Sc, Fe, and Cu (Figure 14). Although a substantial proportion of these elements may bind to the resin, they are typically at low concentrations in most samples of interest, so don't present a major concern. Amberlite IRA 743 is made by the animation of CSDC, itself an anion resin, and it seems likely there may be some residual CSDC which may explain some of this behavior (Popat et al., 1988; Xiao et al., 2003). Other studies have also used the resin for Mo and V separation (Polowczyk et al., 2017) and Se measurement (Bueno & Potin-Gautier, 2002) and the resin is also suggested to bind Alkali and Alkali Earth metals (Cuscurida & Faske, 1991), though the discrepancies between these studies and our findings here may result from differences in loading and elution conditions, which here have been optimized for boron.

## 4. Implications and Outlook

Using our optimized method, within the safe parameter space established above (see Table 1 for summary), we obtain  $\delta^{11}\text{B}$  within error of long-term column values for a range of standards (Table 2), with excellent reproducibility and in some cases representing the best constrained values for these standards. For the synthetic standard NIST 8301f, the batch method has a long-term average of  $14.62 \pm 0.21\text{‰}$  ( $n = 218$ , over 43 sessions at a range of concentrations) or  $14.58 \pm 0.11\text{‰}$  for 20 ppb samples ( $n = 15$ , over 2 sessions), comparable to similarly sized boric acid standards (Figure 15). We also reproduce column values for natural and synthetic carbonates over a wide range of sample matrices and  $\delta^{11}\text{B}$  compositions, including 6 species of planktic foraminifera, 1 species of benthic foraminifera and an in house mixed foraminiferal standard. Synthetic standards are made to represent the composition of a typical foraminifera, coral, coccolithophore and limestone doped with NIST 951 giving them a known boron isotope composition. All of these samples and standards are within error of their defined (for synthetic standards made with NIST 951), published values or values obtained using traditional column chromatography methods, demonstrating the method's robustness (Figure 16).

The batch method offers several advantages over columns. In addition to reduced procedural blanks (Figure 12), it has a faster processing time (12 batch tubes usually takes around 4 hr, whereas 12 columns take 8–10 hr) and the potential to run more samples simultaneously (the number of batch tubes run can easily be doubled to 24, which will take an extra hour). Removing the need for throughflow allows the separation of B from complex matrices which might otherwise clog a gravity column (i.e., samples with organic-rich matrices) and allows control over the time for solution-resin interaction.

Suspending the resin in a solution also allows for a more thorough rinse of the matrix.

Development of the batch method for B purification also has implications for column chemistry. The method development here highlights the need for complete loading for both the batch method and columns to avoid isotopic fractionation. Factors influencing complete sample loading in the batch method, such as ionic strength, sample volume and buffer:acid ratio, likely also play a role in loading for columns and techniques to overcome this such as pre-conditioning the resin with a high pH buffer may similarly aid complete loading in columns. Likewise, mechanisms allowing for lower procedural blanks from the batch may be transferable to columns such as a high pH wash to remove recalcitrant B during resin cleaning.

Overall, the batch method provides a simple and efficient new procedure for B purification for measurement by MC-ICPMS. It offers significant advantages over the traditional gravity column method in both throughput and procedural blank. Its development also highlights aspects of B wet chemistry applicable more widely; we show that if sample loading is not taken to completion the  $\delta^{11}\text{B}$  measured will be fractionated isotopically light, consistent with Rayleigh fractionation, and that complete sample loading requires a balance of sample volume, resin volume, solution ionic strength, and pH. The batch method is an accurate technique for a wide variety of samples and has the potential to improve accessibility and ease for laboratories applying the  $\delta^{11}\text{B}$  pH-proxy.

### Data Availability Statement

Research data underpinning this publication is accessible on the St Andrews Research Repository at (Trudgill et al., 2024) <https://doi.org/10.17630/bb69c2f8-03fc-4b91-82b1-300bac07ac42>.

### Acknowledgments

We thank Allan Watson for helpful discussions. This work was supported by NERC IAPETUS PhD Studentships NE/RO12253/1 to M.T., J.C.B. and E.L., an IAPETUS2 PhD Studentship NE/S007431/1 to C.X.; S.N. was supported by the MOST 111-2116M-002-032-MY3 Grant; J.W.B.R acknowledges support from NERC (Grant NE/N011716/1) and from the European Research Council under the European Union's Horizon 2020 research and innovation program (Grant agreement 805246).

### References

- Aggarwal, J. K., & Palmer, M. R. (1995). Boron isotope analysis. *The Analyst*, 120(5), 1301–1307. <https://doi.org/10.1039/AN9952001301>
- Allison, N., Cole, C., Hintz, C., Hintz, K., Rae, J., & Finch, A. (2018). The effect of ocean acidification on tropical coral calcification: Insights from calcification fluid DIC chemistry. *Chemical Geology*, 497, 162–169. <https://doi.org/10.1016/j.chemgeo.2018.09.004>
- Barker, S., Greaves, M., & Elderfield, H. (2003). A study of cleaning procedures used for foraminiferal Mg/Ca paleothermometry. *Geochemistry, Geophysics, Geosystems*, 4(9), 8407. <https://doi.org/10.1029/2003GC000559>
- Bueno, M., & Potin-Gautier, M. (2002). Solid-phase extraction for the simultaneous preconcentration of organic (selenocystine) and inorganic [Se(IV), Se(VI)] selenium in natural waters. *Journal of Chromatography A*, 963(1–2), 185–193. [https://doi.org/10.1016/s0021-9673\(02\)00125-5](https://doi.org/10.1016/s0021-9673(02)00125-5)
- Cuscurida, M., & Faske, A. J. (1991). 4994627USA.
- De Hoog, C., & Savov, I. (2017). Subduction zones, dehydration, metasomatism, mud and serpentinite volcanoes, and arc magmatism. In H. Marschall & G. Foster (Eds.), *Boron isotopes—The fifth element* (Vol. 7, pp. 219–249). Springer.
- Douville, E., Paterne, M., Cabioch, G., Louvat, P., Gaillardet, J., Juillet-Leclerc, A., & Ayliffe, L. (2010). Abrupt sea surface pH change at the end of the Younger Dryas in the central sub-equatorial Pacific inferred from boron isotope abundance in corals (Porites). *Biogeosciences*, 7(8), 2445–2459. <https://doi.org/10.5194/bg-7-2445-2010>
- Ercolani, C., Lemarchand, D., & Dosseto, A. (2019). Insights on catchment-wide weathering regimes from boron isotopes in riverine material. *Geochimica et Cosmochimica Acta*, 261, 35–55. <https://doi.org/10.1016/j.gca.2019.07.002>
- Foster, G. L. (2008). Seawater pH, pCO<sub>2</sub> and [CO<sub>3</sub><sup>2-</sup>]<sub>3</sub> variations in the Caribbean Sea over the last 130 kyr: A boron isotope and B/Ca study of planktic foraminifera. *Earth and Planetary Science Letters*, 271(1–4), 254–266. <https://doi.org/10.1016/j.epsl.2008.04.015>
- Foster, G. L., Hönisch, B., Paris, G., Dwyer, G. S., Rae, J. W. B., Elliott, T., et al. (2013). Interlaboratory comparison of boron isotope analyses of boric acid, seawater and marine CaCO<sub>3</sub> by MC-ICPMS and NTIMS. *Chemical Geology*, 358, 1–14. <https://doi.org/10.1016/J.CHEMGEO.2013.08.027>
- Foster, G. L., & Rae, J. W. B. (2016). Reconstructing ocean pH with boron isotopes in foraminifera. *Annual Review of Earth and Planetary Sciences*, 44(1), 207–237. <https://doi.org/10.1146/annurev-earth-060115-012226>
- Gagnon, A. C., Gothmann, A. M., Branson, O., Rae, J. W., & Stewart, J. A. (2021). Controls on boron isotopes in a cold-water coral and the cost of resilience to ocean acidification. *Earth and Planetary Science Letters*, 554, 116662. <https://doi.org/10.1016/j.epsl.2020.116662>
- Gutjahr, M., Bordier, L., Douville, E., Farmer, J., Foster, G. L., Hathorne, E. C., et al. (2020). Sub-permil interlaboratory consistency for solution-based boron isotope analyses on marine carbonates. *Geostandards and Geoanalytical Research*, 45(1), ggr.12364. <https://doi.org/10.1111/ggr.12364>
- Hathorne, E. C., Gagnon, A., Felis, T., Adkins, J., Asami, R., Boer, W., et al. (2013). Interlaboratory study for coral Sr/Ca and other element/Ca ratio measurements. *Geochemistry, Geophysics, Geosystems*, 14(9), 3730–3750. <https://doi.org/10.1002/GGGE.20230>
- Hemming, N., & Hanson, G. (1994). A procedure for the isotopic analysis of boron by negative thermal ionization mass spectrometry. *Chemical Geology*, 114(1–2), 147–156. [https://doi.org/10.1016/0009-2541\(94\)90048-5](https://doi.org/10.1016/0009-2541(94)90048-5)
- Hönisch, B., Eggins, S. M., Haynes, L. L., Allen, K. A., Holland, K. D., & Lorbacher, K. (2019). *Boron proxies in paleoceanography and paleoclimatology*. Wiley.
- John, S. G., & Adkins, J. F. (2010). Analysis of dissolved iron isotopes in seawater. *Marine Chemistry*, 119(1–4), 65–76. <https://doi.org/10.1016/j.marchem.2010.01.001>
- Kloppmann, W., Van Houtte, E., Picot, G., Vandenbohede, A., Lebbe, L., Guerrot, C., et al. (2008). Monitoring reverse osmosis treated wastewater recharge into a coastal aquifer by environmental isotopes (B, Li, O, H). *Environmental Science and Technology*, 42(23), 8759–8765. <https://doi.org/10.1021/es801122z>
- Kubota, K., Ishikawa, T., Nagaishi, K., Kawai, T., Sagawa, T., Ikehara, M., et al. (2021). Comprehensive analysis of laboratory boron contamination for boron isotope analyses of small carbonate samples. *Chemical Geology*, 576, 120280. <https://doi.org/10.1016/j.chemgeo.2021.120280>

- Lécuyer, C., Grandjean, P., Reynard, B., Albarède, F., & Telouk, P. (2002).  $^{11}\text{B}/^{10}\text{B}$  analysis of geological materials by ICP-MS plasma 54: Application to the boron fractionation between brachiopod calcite and seawater. *Chemical Geology*, 186(1–2), 45–55. [https://doi.org/10.1016/S0009-2541\(01\)00425-9](https://doi.org/10.1016/S0009-2541(01)00425-9)
- Lemarchand, D., Gaillardet, J., Göpel, C., & Manhès, G. (2002). An optimized procedure for boron separation and mass spectrometry analysis for river samples. *Chemical Geology*, 182(2–4), 323–334. [https://doi.org/10.1016/S0009-2541\(01\)00329-1](https://doi.org/10.1016/S0009-2541(01)00329-1)
- Lloyd, N. S., Sadekov, A. Y., & Misra, S. (2018). Application of  $10^{13}$  ohm Faraday cup current amplifiers for boron isotopic analyses by solution mode and laser ablation multicollector inductively coupled plasma mass spectrometry. *Rapid Communications in Mass Spectrometry*, 32(1), 9–18. <https://doi.org/10.1002/rcm.8009>
- McCulloch, M. T., Holcomb, M., Rankenburg, K., & Trotter, J. A. (2014). Rapid, high-precision measurements of boron isotopic compositions in marine carbonates. *Rapid Communications in Mass Spectrometry*, 28(24), 2704–2712. <https://doi.org/10.1002/rcm.7065>
- Misra, S., Owen, R., Kerr, J., Greaves, M., & Elderfield, H. (2014). Determination of  $\delta^{11}\text{B}$  by HR-ICP-MS from mass limited samples: Application to natural carbonates and water samples. *Geochimica et Cosmochimica Acta*, 140, 531–552. <https://doi.org/10.1016/J.GCA.2014.05.047>
- Muttik, N., Kirsimäe, K., Newsom, H. E., & Williams, L. B. (2011). Boron isotope composition of secondary smectite in suevites at the Ries crater, Germany: Boron fractionation in weathering and hydrothermal processes. *Earth and Planetary Science Letters*, 310(3–4), 244–251. <https://doi.org/10.1016/j.epsl.2011.08.028>
- Polowczyk, I., Cyganowski, P., Urbano, B. F., Rivas, B. L., Bryjak, M., & Kabay, N. (2017). Amberlite IRA-400 and IRA-743 chelating resins for the sorption and recovery of molybdenum(VI) and vanadium(V): Equilibrium and kinetic studies. *Hydrometallurgy*, 169, 496–507. <https://doi.org/10.1016/j.hydromet.2017.02.017>
- Popat, K. M., Anand, P. S., & Dasare, B. D. (1988). Synthesis and characterisation of boron-selective porous condensate cation exchanger. *Reactive Polymers*, 8(2), 143–151. [https://doi.org/10.1016/0167-6989\(88\)90236-x](https://doi.org/10.1016/0167-6989(88)90236-x)
- Rae, J. W. B., Foster, G. L., Schmidt, D. N., & Elliott, T. (2011). Boron isotopes and B/Ca in benthic foraminifera: Proxies for the deep ocean carbonate system. *Earth and Planetary Science Letters*, 302(3–4), 403–413. <https://doi.org/10.1016/J.EPSL.2010.12.034>
- Stewart, J. A., Christopher, S. J., Kucklick, J. R., Bordier, L., Chalk, T. B., Dapoigny, A., et al. (2021). NIST RM 8301 boron isotopes in marine carbonate (simulated coral and foraminifera solutions): Inter-laboratory  $\delta^{11}\text{B}$  and trace element ratio value assignment. *Geostandards and Geoanalytical Research*, 45(1), 77–96. <https://doi.org/10.1111/ggr.12363>
- Trudgill, M., Nuber, S., Block, H. E., Crumpton-Banks, J., Jurikova, H., Little, E., et al. (2024). A simple, low-blank batch purification method for high-precision boron isotope analysis-supporting dataset [Dataset]. *University of St Andrews Research Portal*. <https://doi.org/10.17630/bb69c2f8-03fc-4b91-82b1-300bac07ac42>
- Vengosh, A., Kolodny, Y., Starinsky, A., Chivas, A. R., & McCulloch, M. T. (1991). Coprecipitation and isotopic fractionation of boron in modern biogenic carbonates. *Geochimica et Cosmochimica Acta*, 55(10), 2901–2910. [https://doi.org/10.1016/0016-7037\(91\)90455-e](https://doi.org/10.1016/0016-7037(91)90455-e)
- Vogl, J., & Rosner, M. (2012). Production and certification of a unique set of isotope and delta reference materials for boron isotope determination in geochemical, environmental and industrial materials. *Geostandards and Geoanalytical Research*, 36(2), 161–175. <https://doi.org/10.1111/J.1751-908X.2011.00136.X>
- Wei, H. Z., Lei, F., Jiang, S. Y., Lu, H. Y., Xiao, Y. K., Zhang, H. Z., & Sun, X. F. (2015). Implication of boron isotope geochemistry for the pedogenic environments in loess and paleosol sequences of central China. *Quaternary Research*, 83(1), 243–255. <https://doi.org/10.1016/j.yqres.2014.09.004>
- Xiao, Y.-K., Liao, B.-Y., Liu, W.-G., Xiao, Y., & Swihart, G. H. (2003). Ion exchange extraction of boron from aqueous fluids by Amberlite IRA 743 resin. *Chinese Journal of Chemistry*, 21(8), 1073–1079. <https://doi.org/10.1002/cjoc.20030210819>
- Xu, C., Jurikova, H., Nuber, S., Steele, R. C. J., Trudgill, M., Barker, S., et al. (2024). A rapid, simple, and low-blank pumped ion-exchange column chromatography technique for boron purification from carbonate and seawater matrices. *Geochemistry, Geophysics, Geosystems*, 25(2), e2023GC011228. <https://doi.org/10.1029/2023GC011228>
- Yoshimura, K., Miyazaki, Y., Ota, F., Matsuoka, S., & Sakashita, H. (1998). Complexation of boric acid with the N-methyl-D-glucamine group in solution and in crosslinked polymer. *Journal of the Chemical Society, Faraday Transactions*, 94(5), 683–689. <https://doi.org/10.1039/a707790d>
- Zeebe, R. E., & Rae, J. W. B. (2020). Equilibria, kinetics, and boron isotope partitioning in the aqueous boric acid–hydrofluoric acid system. *Chemical Geology*, 550, 119693. <https://doi.org/10.1016/j.chemgeo.2020.119693>
- Zeininger, H., & Heumann, K. G. (1983). Boron isotope ratio measurement by negative thermal ionization mass spectrometry. *International Journal of Mass Spectrometry and Ion Physics*, 48, 377–380. [https://doi.org/10.1016/0020-7381\(83\)87106-x](https://doi.org/10.1016/0020-7381(83)87106-x)